

Quantum Counting in the Rydberg Blockade

Joseph Gibson,^{1,2} Victor Drouin-Touchette,^{1,2,3} and Stefanos Kourtis^{1,2,4}

¹*Institut quantique, Sherbrooke, Québec, J1K 2R1, Canada*

²*Département de physique, Université de Sherbrooke, Sherbrooke, Québec, J1K 2R1, Canada*

³*Département de génie électrique et de génie informatique,*

Université de Sherbrooke, Sherbrooke, Québec, J1K 2R1, Canada

⁴*Département d'informatique, Université de Sherbrooke, Sherbrooke, Québec, J1K 2R1, Canada*

(Dated: June 25, 2025)

We propose a quantum algorithm for approximately counting the number of solutions to planar 2-satisfiability (2SAT) formulas natively on neutral atom quantum computers. Our algorithm maps Boolean variables to atomic registers arranged in space according to a given formula, so that 2SAT constraints are enforced via the Rydberg blockade between neighboring atoms. A quench under Rydberg dynamics of an initial computational basis state produces a superposition of all solutions after a sufficiently long evolution. For almost uniform superpositions, a polynomial number of measurements is enough to estimate the solution count up to any constant multiplicative factor via sampling based counting. We demonstrate numerically that this protocol leads to almost uniform solution sampling in 1D and 2D grids and that it produces accurate counts for 2SAT instances on punctured grids, suggesting its general applicability as a heuristic for #P-complete problems.

Counting how many objects in a set have a certain property is a fundamental computational task [1]. Counting problems lie at the heart of many interesting applications in artificial intelligence [2–4], network reliability [1, 5], and statistical physics [6, 7], to name a few. However, many counting problems of practical importance are intractable. The computational complexity class #P that encompasses counting contains problems that are thought to be much harder than the hardest problems in the more commonly encountered class NP [1, 8]. An efficient exact algorithm for hard problems in #P could be bootstrapped to solve any problem in the polynomial hierarchy efficiently [9]. The existence of such algorithms is hence considered unlikely.

The improbability of efficient exact algorithms for #P has motivated a great deal of research on solvers that perform well in practice [10]. Exact heuristics have been devised using a variety of techniques, such as component caching [11], knowledge compilation [12], and tensor networks [13, 14]. While these algorithms greatly outperform naive elimination of non-solutions, they are limited to instances with up to a few hundred variables. On the other hand, research on approximate counting, in which we seek only to obtain the solution count up to a multiplicative factor, has produced two families of methods based on either hashing or sampling the solution set. Hashing-based counting involves randomly bisecting the solution set recursively using a hash function family and asking a NP oracle (e.g., a Boolean satisfiability solver) if the hashed set is empty or not [15]. Sampling-based techniques yield an approximate count to #P-complete problems, provided that solutions can be sampled at random almost uniformly [16]. The latter requirement is rather stringent, and hence hashing-based techniques have been more widely adopted to date [10].

It is natural to ask whether quantum computing can

offer improvements in solving counting problems. Early work [17] based on the Grover iteration [18] and recent advances [19–22] do provide an improvement in the black-box setting, but it is unclear whether this persists in practically relevant cases. Moreover, the quantum circuit depths needed to implement these algorithms grows exponentially in the number of variables, thus rendering them inaccessible to noisy quantum processors before fault tolerance [23, 24]. Recently proposed hybrid quantum-classical algorithms for counting [25–27], while more readily implementable in the near term, depend on variational search through high-dimensional parameter spaces that is not guaranteed to converge [28, 29].

In this Letter, we propose a quantum algorithm for counting solutions to planar 2-satisfiability (2SAT) formulas on existing neutral-atom quantum computers (NAQCs). In our algorithm, boolean variables are represented by atomic registers and 2SAT constraints are enforced by the interactions between neighboring atoms. Each iteration consists of (i) initial placement of atoms according to a given 2SAT formula, (ii) quench with a static pulse, and (iii) measurement in the computational basis. We show that, with sufficiently long quenches, our algorithm requires $O(\text{poly}(n))$ operations to perform sampling-based counting on instances with n variables. If we also assume that arbitrary initial computational basis states can be prepared, the measured samples can be used as initial states, leading to a feed-forward (FF) protocol. We demonstrate that this FF protocol returns answers within a constant multiplicative factor of the exact count in polynomial time for partial 2D grid instances. Combined with techniques to implement arbitrary boolean functions on NAQCs [30], our algorithm becomes a powerful heuristic for #P-complete problems.

A NAQC consists of alkaline atoms trapped in optical tweezers and positioned so as to represent a computa-

tional problem. Atoms are then cooled to their electronic ground state. For example, we can consider Rb atoms, whose ground state is $|0\rangle = |5S_{1/2}\rangle$. A laser then coherently drives atoms to the Rydberg state $|1\rangle = |60S_{1/2}\rangle$. Strong dipole-dipole interactions between nearby atoms in the Rydberg state create entanglement and power analog quantum computation and simulation [31, 32].

The dynamics of a register of n trapped atoms is described as evolution under the Rydberg Hamiltonian [33]

$$H_{\text{Ryd}}(\Omega) = \sum_{i=1}^n \frac{\Omega}{2} X_i + \sum_{i<j}^n V_{ij} n_i n_j, \quad (1)$$

where $X_i = |1_i\rangle\langle 0_i| + |0_i\rangle\langle 1_i|$ describes Rabi oscillations between ground (excited) state $|0_i\rangle$ ($|1_i\rangle$) at atom i at the resonance frequency Ω , $V_{ij} \approx C_6 r_{ij}^{-6}$ is the interaction between atoms i and j in the Rydberg state at distance r_{ij} with $C_6 > 0$, and $n_i = |1_i\rangle\langle 1_i|$.

In the limit $V_{ij} \gg \Omega$, called the Rydberg blockade, pairs of atoms within a distance smaller than the blockade radius $r_B = (C_6/\Omega)^{1/6}$ are energetically prohibited to simultaneously transition from ground state to Rydberg state. Given the sharp decay of interactions with distance, the atomic array can thus effectively be seen as a so-called unit-disk graph $G = (V, E)$, where the i -th atom is represented by vertex $i \in V$ ($|V| = n$) and pairs of atoms i and j with $r_{ij} < r_B$ are connected by an edge $(i, j) \in E$. In this limit, the Rydberg Hamiltonian is approximately equal to the PXP Hamiltonian [34, 35]

$$H_{\text{PXP}}(G, \Omega) = \Omega \sum_{i \in V} X_i \prod_{(i,j) \in E} P_j, \quad (2)$$

with $P_j = \frac{1-\sigma_j^z}{2} = \mathbb{1} - |1_j\rangle\langle 1_j|$. The PXP Hamiltonian captures the low-energy dynamics in the Rydberg blockade, where evolution is restricted within the common $+1$ eigenspace of all projectors, namely, the states $\{|0\rangle_i |0\rangle_j, |0\rangle_i |1\rangle_j, |1\rangle_i |0\rangle_j\}$ for $(i, j) \in E$. The state $|0\rangle^{\otimes n}$ with all atoms relaxed to their ground state, in which NAQCs are typically initialized, is a $+1$ eigenstate of all projectors. The residual long-range tail of the interactions (i.e., V_{ij} for $(i, j) \notin E$) can be arbitrarily suppressed by forming ‘‘logical’’ Rydberg atoms that incur only polynomial overheads in system size [36–39]. We therefore adopt Eq. (2) for our purposes below.

The Rydberg blockade allows direct access to the solution space of a family of 2SAT formulas. If we denote the computational basis states of two neighboring atoms within a blockade radius as $|x_i x_j\rangle$, where $x_i, x_j = 0, 1$ are Boolean variables, we see that low-energy states satisfy the constraint $\neg x_i \vee \neg x_j$, where \neg is the negation operation $\neg x_i = 1 - x_i$. Therefore, every component $|x\rangle = |x_n \dots x_1\rangle$ of a low-energy state in the Rydberg blockade is a solution to a monotone 2SAT formula

$$\phi_G(x) = \bigwedge_{(i,j) \in E} (\neg x_i \vee \neg x_j), \quad (3)$$

defined for a given blockade graph G . Computing the number of solutions $|\phi_G(x)| = |\{x : \phi_G(x) = 1\}|$ of arbitrary monotone 2SAT formulas is $\#P$ -complete, i.e., as hard as the hardest problems in class $\#P$ [1], and remains so even for planar 3-regular bipartite graphs [40].

To design a quantum algorithm for counting, we exploit a well-known correspondence between almost uniform sampling and approximate counting, first operationalized in a classical algorithm by Jerrum, Valiant, and Vazirani (JVV) [16]. The JVV algorithm samples solutions to a given problem, and then fixes variables based on their observed maximum likelihood in the sample. The variable fixing defines the subproblem to sample from at the following step. This process of variable-fixing is called self-reduction and continues until all variables have been fixed [41]. An estimate of the solution count is computed from the product of all observed maximum likelihoods. There are two requirements for the estimate to be within a constant multiplicative factor of the exact count: the problem needs to be self-reducible, and solutions need to be sampled sufficiently uniformly.

A boolean formula ϕ is self-reducible if a solution can be constructed out of solutions to subformulas of the problem, where the subformulas are defined by fixing boolean variables. This can be expressed as

$$\phi(x) = 1 \Leftrightarrow \{\phi(x|x_i = 1) = 1\} \vee \{\phi(x|x_i = 0) = 1\}. \quad (4)$$

All SAT problems are self-reducible [42], and the first requirement is hence satisfied in our case.

To assess whether a solution sampler is sufficiently uniform, we can compare its distribution D with the uniform distribution Q over the set of all solutions $\mathcal{X} = \{x | \phi(x) = 1\}$. One way to quantify the sampler non-uniformity is via the total variation distance as [43]

$$\eta(D) = \|D - Q\|_{\text{TV}} = \frac{1}{2} \sum_{x \in \mathcal{X}} |D(x) - Q(x)|. \quad (5)$$

A sampling-based counter that returns estimates within a constant factor of the exact count for any instance size requires $n\eta = O(1)$ [16].

We now ask whether these requirements can be satisfied in NAQCs. First, we show that this representation of 2SAT problems preserves self-reducibility. Suppose that in the self-reduction process we wish to fix the c -th variable to $x_c = 0$. On a NAQC, we must fix $|x_c\rangle = |0\rangle$. According to (2), an atom in its ground state does not constrain the state of its first neighbors in $G = (V, E)$. We can therefore equivalently represent the reduced instance with an array that simply omits atom c altogether, that is, the induced subgraph $G' = (V', E')$ with $V' = V \setminus c$. On the other hand, suppose that we fix $x_c = 1$. This choice forces the *first* neighbors of c to be in $|0\rangle$, which in turn means that the *second* neighbors of c are unconstrained by the choice $|x_c\rangle = |1\rangle$. We can therefore represent the reduced instance with an array that omits

Algorithm 1 RYDCOUNT

Input: R : atom register expressing $\phi_G(x)$ as the blockade graph $G = (V, E)$
 Ω : Rabi frequency
 n_{samp} : number of samples taken at each step
 $t_{\text{min}}, t_{\text{max}}$: minimum and maximum evolution times
 $\kappa \leftarrow 1$

- 1: **repeat**
- 2: $\sigma \leftarrow \{\}$
- 3: $|\psi_0\rangle \leftarrow |0\rangle^{\otimes |V|}$
- 4: **for** $1, n_{\text{samp}}$ **do** ▷ This is RYDSAMP
- 5: $t_{\text{rand}} \xleftarrow{\text{sample}} U(t_{\text{min}}, t_{\text{max}})$ ▷ U : uniform dist.
- 6: Initialize register R in state $|\psi_0\rangle$
- 7: $x \xleftarrow{\text{measure}} \exp[-iH_{\text{Ryd}}(\Omega)t_{\text{rand}}]|\psi_0\rangle$
- 8: σ append x
- 9: $(|\psi_0\rangle \leftarrow |x\rangle)$ ▷ For Feed-Forward only
- 10: **end for**
- 11: $p_i \leftarrow \frac{1}{n_{\text{samp}}} \sum_{x \in \sigma} x_i$ ▷ likelihood of x_i
- 12: $c \leftarrow \text{argmax}_i(p_i)$
- 13: $R \leftarrow R(x|x_c = 1)$ ▷ Reduce the register
- 14: $R \leftarrow R(x|x_j = 0 \forall (c, j) \in E)$ ▷ Reduce the register
- 15: $\kappa \leftarrow \frac{\kappa}{p_c}$
- 16: **until** $x_i \leftarrow \{0, 1\} \forall i \in V$

Output: Estimated count = κ

atom c and its first neighbors, i.e., $G'' = (V'', E'')$ with $V'' = V \setminus (c \cup \{j|(c, j) \in E\})$.

The next question is how uniformly we can sample solutions using a Rydberg processor. This question is open-ended, since one can devise many protocols to explore the constrained Hilbert space of (2). Here we will focus solely on quenching an atomic register initialized in a product state with $\mathcal{U}_{\text{PXP}}(t) = e^{-iH_{\text{PXP}}t}$. For all but an $O(1)$ subset of initial states that exhibit unexpectedly long thermalization times [44–46], \mathcal{U}_{PXP} is chaotic [45, 47–49]. In the unattainable limit $t \rightarrow \infty$, evolution of generic initial states thus yields equal superpositions of solutions. A more useful lower bound on the evolution time needed for close-to-uniform sampling is the Thouless time t_{Th} [50]. We study t_{Th} numerically for the PXP model in the SM. In practice, the qubit coherence of near-term NAQCs upper-bounds evolution times. While we do not have theoretical guarantees of uniformity at these timescales for specific initial states, below we demonstrate numerically that quenches of simple states can produce samples that are sufficiently uniform for approximate counting.

We now introduce RYDCOUNT, a sampling-based counting algorithm for NAQCs, as described in Algorithm 1. RYDCOUNT takes as input the register R that defines a 2SAT instance in its blockade graph, number of samples n_{samp} , Hamiltonian parameters (Rabi frequency Ω), and evolution time bounds $t_{\text{min}}, t_{\text{max}}$. The gist of RYDCOUNT is repeated iterations of a subroutine we call RYDSAMP, which is preparation and measurement of the state $|\psi_t\rangle = \exp[-iH_{\text{Ryd}}(\Omega)t_{\text{rand}}]|\psi_0\rangle$ at time $t = t_{\text{rand}}$ taken uniformly at random in the time interval

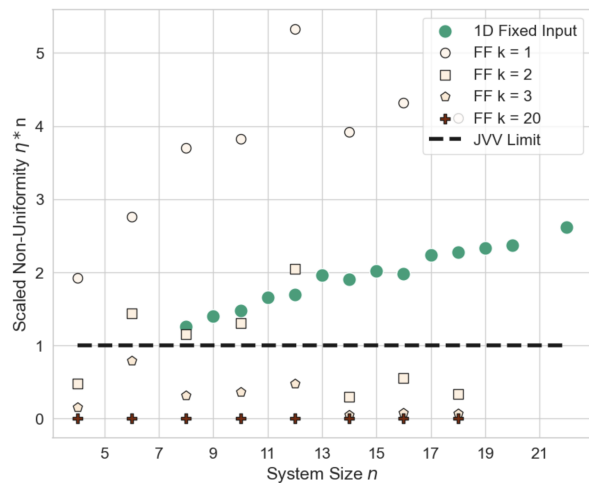


FIG. 1. Scaled non-uniformity $n\eta$ of RYDSAMP as a function of system size n . The dashed line illustrates $n\eta = O(1)$, required for a constant-factor approximation. Data is shown for 1D chains for the FI (green) and FF protocols. The FF data is shown for different values of k (different symbols), showing a convergence to a uniform distribution.

$[t_{\text{min}}, t_{\text{max}}]$ [51]. Once samples are obtained (steps 3–10), we calculate the variable x_c that is most likely to be 1 (step 11 and 12). In the subsequent rounds of sampling this variable is fixed to 1, so we remove the corresponding atom (step 13) and all its neighbors (step 14) from the register, as discussed. Finally, the estimated count κ is updated (step 15) until all variables are set (step 16).

We characterize RYDSAMP by numerically simulating evolution under H_{Ryd} with interactions restricted to nearest neighbors [52]. We set $\Omega = 1$, $V_{ij} = 50$, $t_{\text{min}} \sim 10\Omega^{-1}$, and $t_{\text{max}} \sim 10^3\Omega^{-1}$. In what we call the fixed-input (FI) protocol, we fix the initial state for RYDSAMP to $|\psi_0\rangle = |0\rangle^{\otimes n}$ at every iteration. Fig. 1 shows the scaled non-uniformity $n\eta$ for 1D chains with open boundary conditions. We find that $n\eta$ scales roughly linearly with n , indicating biased sampling. This is due to atypical low-Hamming weight states with high survival probability. We characterize this effect in the SM.

To mitigate this bias, we propose a *feed-forward* (FF) protocol for RYDCOUNT. The initial state is again $|0\rangle^{\otimes n}$, but after each iteration of RYDSAMP, the measured bitstring is fed in as the new initial state (optional step 9 in Algorithm 1). This requires the NAQC to be initialized in an arbitrary computational state, which can be achieved with limited local control [53, 54]. The non-uniformity of this protocol is also shown in Fig. 1. For all 1D chain instances tested, η goes to zero as the number of FF steps, k , increases. This indicates that RYDSAMP can be brought arbitrarily close to a uniform distribution.

Next, we perform end-to-end benchmarks of RYDCOUNT. While the FF protocol is promising, the large number of evolutions it requires is prohibitive for classical simulations. For validation of RYDCOUNT, we in-

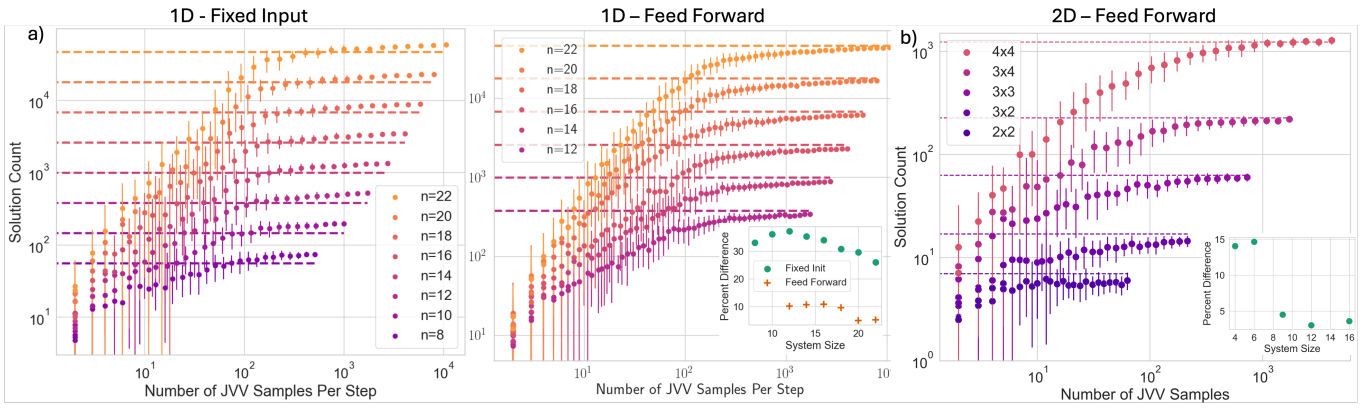


FIG. 2. Accuracy of RYDCOUNT as a function of n_{samp} for (a) 1D chains of length n and (b) 2D grids of size $n = L_x \times L_y$. Dashed lines represent exact counts. Insets show the relative error between estimated and exact counts versus n . In (a), the left (right) panel shows results for the FI (practical FF) protocol.

stead use a more practical FF protocol where many samples are gathered at each step, and all samples collected are used in the count. Again, for all instances tested, $n\eta = O(1)$ (see SM), indicating that the practical FF also leads to almost uniform sampling. To assess convergence, we compare to the exact count as a function of the number of samples n_{samp} taken at each step. For 1D, the number of solutions is known to increase as the Fibonacci sequence [45]. Results are shown in Fig. 2(a) for FI (left) and FF (right) protocols. The inset displays a decreasing relative error as n grows. The FI protocol systematically overshoots the expected value. This is a consequence of the bias towards low-Hamming weight states discussed above. The FF protocol mitigates this bias. We then apply RYDCOUNT with the FF protocol on 2D square grids in Fig. 2(b), where a classical counter is used to obtain an exact solution [55]. The inset shows similar convergence as in 1D. For the largest system, the error is below 5%, an improvement over the 1D chain of similar length. In both the 1D and 2D settings and for both FI and FF, RYDCOUNT converges as $n_{\text{samp}} \rightarrow n^4$, which is consistent with the theoretical worst-case bound $O(n^4)$ [16, 43, 56]. Note also that the estimated count for the largest systems exceeds the number of samples taken, indicating an efficiency gain even in the small instances accessible in classical numerics.

Finally, we turn to non-trivial #2SAT instances defined on punctured square grids. Fig. 3 shows convergence to solution with less than $\sim 10\%$ error for polynomially scaling n_{samp} . While the complexity of #2SAT for this ensemble is unknown to us, the similar ensemble of planar 3-regular bipartite graphs is #P-complete [40]. Also, the fact that any boolean function can be represented as 2D atomic registers [30, 36] implies that RYDCOUNT can approximate any #P function.

The FI protocol of RYDCOUNT does not require selective addressability or hyperfine states and is thus im-

plementable in existing analog NAQCs with only global pulse control. Analog protocols can access longer evolution times compared to digital devices in the near-term, given current noise levels and trotterization errors in the latter [57]. As an example, Ref. [58] reached $\Omega t_{\text{max}} \sim 8$ for a digital implementation of a quench on a 1D chain of $n = 28$ qubits, whereas NAQCs operating in analog simulation mode can access $\Omega t_{\text{max}} \sim 24$ [59]. Improvements to classical sampling-based counting that also allow for biased sampling [43, 60, 61] directly apply to RYDCOUNT. RYDCOUNT requires no parameter optimization, thereby sidestepping obstacles to variational quantum algorithms. Finally, its validity (though not its runtime) is inherently resilient to noise, since the solutions sampled can be verified in linear time.

While RYDCOUNT, in its basic form, can be imple-

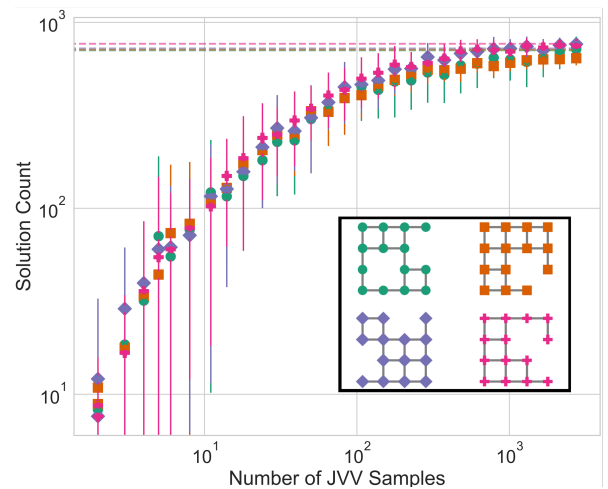


FIG. 3. Performance of RYDCOUNT (practical FF protocol) for a selection of 2D punched grids. Dashed lines represent exact counts. The inset shows the chosen punched grids with matching colors/markers.

mented on NAQCs today, short-term hardware improvements can make it competitive to state-of-the-art classical heuristics for $\#P$ problems. First, although the clock rate of NAQCs is currently less than 10 Hz [62, 63], rates of 100 Hz or higher are achievable [64]. Second, current NAQCs have hundreds of qubits [62, 63], whereas $\#SAT$ instances start challenging state-of-the-art classical solvers at several hundred to a few thousand variables. Trapping and rearrangement of registers of thousands of atoms has already been demonstrated [65, 66]. Third, while the current maximum sequence duration in NAQCs is $t_{\max} = 6 \mu s$ [62, 63], improvements in trapping, cooling, and lasing can increase it drastically [59]. Finally, the FF protocol and mitigation strategies for unwanted long-range interaction tails require selective addressability of atoms, which is already implemented in academic NAQCs [54, 67, 68].

This research was financially supported by Prompt through its *Soutien aux organismes de recherche* program, by the Natural Sciences and Engineering Research Council of Canada (NSERC) through an Alliance grant, and by Pasqal Canada through its contribution to the Institutional Research Chair in Quantum Artificial Intelligence at Université de Sherbrooke.

-
- [1] L. G. Valiant, *SIAM Journal on Computing* **8**, 410–421 (1979).
- [2] D. Roth, *Artificial Intelligence* **82**, 273–302 (1996).
- [3] T. Sang, P. Bearne, and H. Kautz, in *Proceedings of the 20th National Conference on Artificial Intelligence*, Vol. 1 (2005) pp. 475–481.
- [4] T. Baluta, S. Shen, S. Shinde, K. S. Meel, and P. Saxena, in *Proceedings of the 2019 ACM SIGSAC Conference on Computer and Communications Security*, CCS ’19 (Association for Computing Machinery, New York, NY, USA, 2019) p. 1249–1264.
- [5] L. Duenas-Osorio, K. Meel, R. Paredes, and M. Vardi, *Proceedings of the AAAI Conference on Artificial Intelligence* **31** (2017), 10.1609/aaai.v31i1.11178.
- [6] S. Nagy, R. Paredes, J. M. Dudek, L. Dueñas-Osorio, and M. Y. Vardi, *Physical Review E* **109** (2024), 10.1103/physreve.109.055301.
- [7] M. Jerrum and A. Sinclair, *SIAM Journal on Computing* **22**, 1087–1116 (1993).
- [8] L. Valiant, *Theoretical Computer Science* **8**, 189 (1979).
- [9] S. Toda, *SIAM Journal on Computing* **20**, 865 (1991), <https://doi.org/10.1137/0220053>.
- [10] C. P. Gomes, A. Sabharwal, and B. Selman, in *Handbook of satisfiability* (IOS press, 2021) pp. 993–1014.
- [11] T. Sang, F. Bacchus, P. Beame, H. A. Kautz, and T. Pitassi, *SAT* **4**, 7th (2004).
- [12] J.-M. Lagniez and P. Marquis, in *Proceedings of the Twenty-Sixth International Joint Conference on Artificial Intelligence, IJCAI-17* (2017) pp. 667–673.
- [13] S. Kourtis, C. Chamon, E. R. Mucciolo, and A. E. Ruckenstein, *SciPost Phys.* **7**, 060 (2019).
- [14] J. M. Dudek, L. Dueñas-Osorio, and M. Y. Vardi, “Efficient Contraction of Large Tensor Networks for Weighted Model Counting through Graph Decompositions,” (2020), [arXiv:1908.04381 \[cs\]](https://arxiv.org/abs/1908.04381).
- [15] L. Stockmeyer, *SIAM Journal on Computing* **14**, 849 (1985), <https://doi.org/10.1137/0214060>.
- [16] M. R. Jerrum, L. G. Valiant, and V. V. Vazirani, *Theoretical Computer Science* **43**, 169 (1986).
- [17] G. Brassard, P. Høyer, and A. Tapp, in *Automata, Languages and Programming*, edited by K. G. Larsen, S. Skyum, and G. Winskel (Springer Berlin Heidelberg, Berlin, Heidelberg, 1998) pp. 820–831.
- [18] L. K. Grover, in *Proceedings of the twenty-eighth annual ACM symposium on Theory of computing - STOC ’96*, STOC ’96 (ACM Press, 1996) p. 212–219.
- [19] S. Aaronson and P. Rall, “Quantum approximate counting, simplified,” in *Symposium on Simplicity in Algorithms* (Society for Industrial and Applied Mathematics, 2020) p. 24–32.
- [20] S. Aaronson, R. Kothari, W. Kretschmer, and J. Thaler, in *35th Computational Complexity Conference (CCC 2020)*, Leibniz International Proceedings in Informatics (LIPIcs), Vol. 169, edited by S. Saraf (Schloss Dagstuhl–Leibniz-Zentrum für Informatik, Dagstuhl, Germany, 2020) pp. 7:1–7:47.
- [21] A. Belovs and A. Rosmanis, “Tight quantum lower bound for approximate counting with quantum states,” (2024), [arXiv:2002.06879 \[quant-ph\]](https://arxiv.org/abs/2002.06879).
- [22] W. Kretschmer, “QMA lower bounds for approximate counting,” (2019), [arXiv:1902.02398 \[cs.CC\]](https://arxiv.org/abs/1902.02398).
- [23] E. Stoudenmire and X. Waintal, *Physical Review X* **14** (2024), 10.1103/physrevx.14.041029.
- [24] S. Lee and S. Y. Nam, *Ieee Access* **12**, 43027 (2024).
- [25] J. Drapeau, S. Banerjee, and S. Kourtis, “Counting with the quantum alternating operator ansatz,” (2025), [arXiv:2503.07720 \[quant-ph\]](https://arxiv.org/abs/2503.07720).
- [26] Z. Zhang, R. Paredes, B. Sundar, D. Quiroga, A. Kyriilidis, L. Duenas-Osorio, G. Pagano, and K. R. A. Hazzard, *Quantum Science and Technology* **10**, 015022 (2024).
- [27] B. Sundar, R. Paredes, D. T. Damanik, L. Dueñas-Osorio, and K. R. A. Hazzard, “A quantum algorithm to count weighted ground states of classical spin Hamiltonians,” (2019), [arXiv:1908.01745 \[quant-ph\]](https://arxiv.org/abs/1908.01745).
- [28] L. Bittel and M. Kliesch, *Phys. Rev. Lett.* **127**, 120502 (2021).
- [29] M. Larocca, S. Thanasilp, S. Wang, K. Sharma, J. Biamonte, P. J. Coles, L. Cincio, J. R. McClean, Z. Holmes, and M. Cerezo, “A review of barren plateaus in variational quantum computing,” (2024), [arXiv:2405.00781 \[quant-ph\]](https://arxiv.org/abs/2405.00781).
- [30] S. Stastny, H. P. Büchler, and N. Lang, *Physical Review B* **108**, 085138 (2023), [arXiv:2301.01508 \[cond-mat, physics:physics, physics:quant-ph\]](https://arxiv.org/abs/2301.01508).
- [31] K. Wintersperger, F. Dommert, T. Ehmer, A. Houranov, J. Klepsch, W. Mauerer, G. Reuber, T. Strohm, M. Yin, and S. Luber, *EPJ Quantum Technology* **10**, 32 (2023).
- [32] A. Browaeys and T. Lahaye, *Nature Physics* **16**, 132–142 (2020).
- [33] Here we assume that the driving laser is tuned exactly to the resonance between ground and Rydberg states. We therefore omit the detuning term that commonly appears in the Rydberg Hamiltonian.
- [34] I. Lesanovsky, *Phys. Rev. Lett.* **106**, 025301 (2011).

- [35] S. Ji, C. Ates, and I. Lesanovsky, *Phys. Rev. Lett.* **107**, 060406 (2011).
- [36] H. Pichler, S.-T. Wang, L. Zhou, S. Choi, and M. D. Lukin, arXiv preprint arXiv:1809.04954 (2018).
- [37] M.-T. Nguyen, J.-G. Liu, J. Wurtz, M. D. Lukin, S.-T. Wang, and H. Pichler, *PRX Quantum* **4**, 010316 (2023).
- [38] M. Lanthaler, K. Ender, C. Dlaska, and W. Lechner, arXiv preprint arXiv:2410.03902 (2024).
- [39] L. Bombieri, Z. Zeng, R. Tricarico, R. Lin, S. Notarnicola, M. Cain, M. D. Lukin, and H. Pichler, *PRX Quantum* **6**, 020306 (2025).
- [40] M. Xia and W. Zhao, in *International Conference on Theory and Applications of Models of Computation* (Springer, 2006) pp. 356–364.
- [41] A visual representation of the self-reduction process can be found in Ref. [43].
- [42] L. A. Hemaspaandra, “The power of self-reducibility: Selectivity, information, and approximation,” (2019), arXiv:1902.08299 [cs.CC].
- [43] C. Moore and S. Mertens, *The Nature of Computation* (Oxford University Press, 2011).
- [44] H. Bernien, S. Schwartz, A. Keesling, H. Levine, A. Omran, H. Pichler, S. Choi, A. S. Zibrov, M. Endres, M. Greiner, V. Vuletić, and M. D. Lukin, *Nature* **551**, 579–584 (2017).
- [45] C. J. Turner, A. A. Michailidis, D. A. Abanin, M. Serbyn, and Z. Papić, *Phys. Rev. B* **98**, 155134 (2018).
- [46] D. Bluvstein, A. Omran, H. Levine, A. Keesling, G. Semeghini, S. Ebadi, T. T. Wang, A. A. Michailidis, N. Maskara, W. W. Ho, *et al.*, *Science* **371**, 1355 (2021).
- [47] J. Choi, A. L. Shaw, I. S. Madjarov, X. Xie, R. Finkelstein, J. P. Covey, J. S. Cotler, D. K. Mark, H.-Y. Huang, A. Kale, *et al.*, *Nature* **613**, 468 (2023).
- [48] W. W. Ho, S. Choi, H. Pichler, and M. D. Lukin, *Physical Review Letters* **122** (2019), 10.1103/physrevlett.122.040603.
- [49] M. Schnee, R. Radgohar, and S. Kourtis, arXiv preprint arXiv:2406.12968 (2024).
- [50] M. Schiulaz, E. J. Torres-Herrera, and L. F. Santos, *Phys. Rev. B* **99**, 174313 (2019).
- [51] Note that the sampled times t_{rand} are discarded if they are closer than the Heisenberg time t_H . This reduces inter-correlations between samples [69].
- [52] All calculations were performed using the QuSpin library [70] on an AMD EPYC 7F72 CPU with 100GB of RAM available.
- [53] K. Goswami, R. Mukherjee, H. Ott, and P. Schmelcher, *Physical Review Research* **6**, 023031 (2024).
- [54] A. de Oliveira, E. Diamond-Hitchcock, D. Walker, M. Wells-Pestell, G. Pelegri, C. Picken, G. Malcolm, A. Daley, J. Bass, and J. Pritchard, *PRX Quantum* **6**, 010301 (2025).
- [55] A. Ignatiev, A. Morgado, and J. Marques-Silva, in *SAT* (2018) pp. 428–437.
- [56] C. P. Gomes, J. Hoffmann, A. Sabharwal, and B. Selman, in *Proceedings of the 20th International Joint Conference on Artificial Intelligence, IJCAI’07* (Morgan Kaufmann Publishers Inc., San Francisco, CA, USA, 2007) p. 2293–2299.
- [57] A. J. Daley, I. Bloch, C. Kokail, S. Flannigan, N. Pearson, M. Troyer, and P. Zoller, *Nature* **607**, 667 (2022).
- [58] J.-Y. Desautels, E. J. Gustafson, A. C. Li, Z. Papić, and J. C. Halimeh, *Physical Review A* **110**, 042606 (2024).
- [59] L. Leclerc, *Quantum computing with Rydberg atoms: control and modelling for quantum simulation and practical algorithms*, Ph.D. thesis, Université Paris-Saclay (2024).
- [60] A. Sinclair and M. Jerrum, *Information and Computation* **82**, 93 (1989).
- [61] C. P. Gomes, J. Hoffmann, A. Sabharwal, and B. Selman, in *IJCAI*, Vol. 2007 (2007) pp. 2293–2299.
- [62] Pasqal, “Technical overview for advanced users orion beta,” (2025).
- [63] J. Wurtz, A. Bylinskii, B. Braverman, J. Amato-Grill, S. H. Cantu, F. Huber, A. Lukin, F. Liu, P. Weinberg, J. Long, S.-T. Wang, N. Gemelke, and A. Keesling, “Aquila: Quera’s 256-qubit neutral-atom quantum computer,” (2023), arXiv:2306.11727 [quant-ph].
- [64] C. Dalyac, L. Leclerc, L. Vignoli, M. Djellabi, W. d. S. Coelho, B. Ximenez, A. Dareau, D. Dreon, V. E. Elfving, A. Signoles, *et al.*, *The European Physical Journal A* **60**, 177 (2024).
- [65] H. J. Manetsch, G. Nomura, E. Bataille, K. H. Leung, X. Lv, and M. Endres, “A tweezer array with 6100 highly coherent atomic qubits,” (2024), arXiv:2403.12021 [quant-ph].
- [66] G. Pichard, D. Lim, É. Bloch, J. Vaneecloo, L. Bourachot, G.-J. Both, G. Mériaux, S. Dutartre, R. Hostein, J. Paris, *et al.*, *Physical Review Applied* **22**, 024073 (2024).
- [67] D.-S. Xiang, Y.-W. Zhang, H.-X. Liu, P. Zhou, D. Yuan, K. Zhang, S.-Y. Zhang, B. Xu, L. Liu, Y. Li, *et al.*, arXiv preprint arXiv:2410.15455 (2024).
- [68] G. Bornet, G. Emperauger, C. Chen, F. Machado, S. Chern, L. Leclerc, B. Gély, Y. T. Chew, D. Barredo, T. Lahaye, N. Y. Yao, and A. Browaeys, *Phys. Rev. Lett.* **132**, 263601 (2024).
- [69] A. K. Das, C. Cianci, D. G. A. Cabral, D. A. Zarate-Herrada, P. Pinney, S. Pilatowsky-Cameo, A. S. Matsoukas-Roubeas, V. S. Batista, A. del Campo, E. J. Torres-Herrera, and L. F. Santos, *Phys. Rev. Res.* **7**, 013181 (2025).
- [70] P. Weinberg and M. Bukov, *SciPost Phys.* **7**, 020 (2019).
- [71] L. Accardi, *Physics Reports* **77**, 169 (1981).

Effective probability distribution of RydSamp

We wish to calculate the probability distribution $D(x)$ that RYDSAMP samples from.

In the case of the FI protocol, we proceed thusly. After random $t_{\text{rand}} \in U(t_{\text{min}}, t_{\text{max}})$ are chosen, we simulate the evolution of the initial state up to the maximum t_{rand} sampled, while computing and storing the average probability mass function at each t_{rand} . This effective probability distribution is then stored and classically sampled to simulate RYDSAMP. For an initially fixed input state $|\psi_s\rangle$, the distribution of the output states is

$$D(x) = \frac{|\langle x | e^{-iH_{\text{Ryd}} t_{\text{rand}}} | \psi_s \rangle|^2}{\text{Tr}(P_x \mathcal{U}(t_{\text{rand}}) \rho_s \mathcal{U}^\dagger(t_{\text{rand}}))}, \quad (6)$$

where x is a computational basis state (i.e., a solution to the 2SAT problem), averaging is over random t_{rand} . In the second line we describe an equivalent formulation based on the density matrix formalism, where $\mathcal{U}(t_{\text{rand}}) =$

$e^{-iH_{\text{Ryd}}t_{\text{rand}}}$ is the unitary evolution under the Rydberg Hamiltonian at a random time t_{rand} , ρ_s is the density matrix defined by the initial state $|\psi_s\rangle$, and P_x is the projection operator over x . For the FI protocol described in the text, we always choose $|\psi_s\rangle = |0\rangle^{\otimes n}$.

The impetus for the FF protocol is to mitigate the bias towards low-Hamming weight states seen in the FI protocol. The ideal protocol that would achieve this would be to design a quantum Markov chain [71], with (memoryless) transition map \mathcal{U} (describing both the evolution for a random time and the measurement process) and initial state $|0\rangle^{\otimes n}$. The output distribution after k steps can be described as

$$D_k(x) = \text{Tr}(P_x \mathcal{U} \rho_{k-1} \mathcal{U}^\dagger), \quad (8)$$

$$\rho_{k-1} = \sum_{x \in \mathcal{X}} D_{k-1}(x) |x\rangle\langle x|. \quad (9)$$

where ρ_k is the post-measurement density operator at the k -th step, and $\rho_0 = |0\rangle^{\otimes n} \langle 0|^{\otimes n}$. Ideally, if the chain is mixing, $D_k(x)$ should converge to the uniform distribution, i.e. $\rho_k \rightarrow \frac{\mathbb{1}}{|\mathcal{X}|}$ as $k \rightarrow \infty$.

The FF protocol as described above is impractical to implement when benchmarking RYDCOUNT, as it relies on multiple evolutions of the density matrix. To validate FF at larger scale, we outlined in the main text a more practical protocol, which we detail here. In this practical FF protocol, the input state for the next step of FF is a single computational state sampled from D_{k-1} , i.e. $\rho_{k-1} = |x\rangle\langle x|$. We also do not discard samples, as it is more efficient experimentally and computationally to extract M shots of the same unitary evolution than 1 shot of M different unitary evolutions. If we assume that both the vanilla and the practical versions of FF perform evolutions until equilibration under a chaotic Hamiltonian, the computational cost of classically simulating these evolutions scales exponentially with system size in both cases. On the other hand, the practical FF requires polynomially fewer of these evolutions and thus is more amenable to classical simulation for the system sizes considered.

Thus, in the implementation of the practical FF, we combine all the observed samples from each of the k evolutions, resulting in an overall distribution $\mathcal{D}(k)$. An equivalent way of getting a similar population sample would be to evolve a mixed state, ρ_m , that is equal to the normalized sum of all the chosen pure initial states $\rho_m = \frac{1}{k} \sum_s \rho_s$. Note that each initial state at each step is still linked to the previous measurement outcome, as in the quantum Markov chain proposal described above.

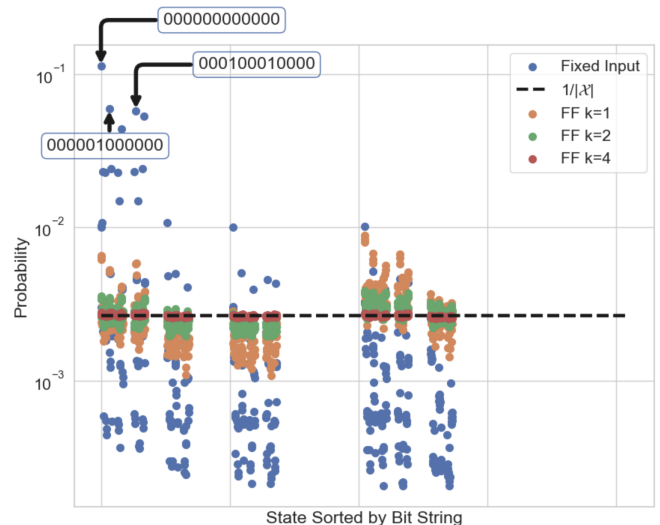


FIG. 4. Comparison of the probability distributions for all bitstrings for a 1D chain of $n = 18$ atoms for the FI (blue) and FF (orange, green and red, for different number of FF steps k) protocols and the $\frac{1}{|\mathcal{X}|}$ limit (dashed black line). We highlight the 3 bit strings with the largest probabilities from each distribution. Large white gaps correspond to non-valid solutions, which are bitstrings that were never obtained.

Characteristics of RydSamp distribution under fixed-input and feed-forward evolution

We now numerically probe the properties of the output distribution of RYDSAMP. Simulations are done directly on the PXP model, i.e., the $V \gg \Omega$ limit of the Rydberg Hamiltonian. The raw distribution for a 1D chain, $n = 18$, over all 2^n bit strings is shown in Fig. 4. Only the states that obey the 2SAT constraints (i.e., respecting the nearest neighbor blockade condition) have a non-zero probability. For the FI procedure, there is a small number of exceptional points with atypically high probability.

For 1D chains of length n , we show in Fig. 5 the averaged survival probability

$$S_p(t) = |\langle \psi_0 | \mathcal{U}_{PXP}(t) | \psi_0 \rangle|^2 \quad (10)$$

of the $|\psi_0\rangle = |0\rangle^{\otimes n}$ state, averaged over many random long times t_{rand} . The scaling of the averaged $S_p(t)$ indicates that the occupation of the initial state $|\psi_0\rangle$ is exponentially (in n) larger than the expected thermal value of $\frac{1}{|\mathcal{X}|}$. This is seen for all initial computational basis states, but it is most prominent with $|0\rangle^{\otimes n}$. While this may at first seem to be detrimental to our sampling scheme, we find that, for the $|0\rangle^{\otimes n}$ initial state, this exponential separation occurs only for configurations with low Hamming weight of $O(1)$ (e.g., $|00 \dots 010 \dots 00\rangle$).

The practical FF procedure mitigates this bias towards low Hamming weight states, because the variety of initial states averages out exceptional points. In Fig. 6, we show

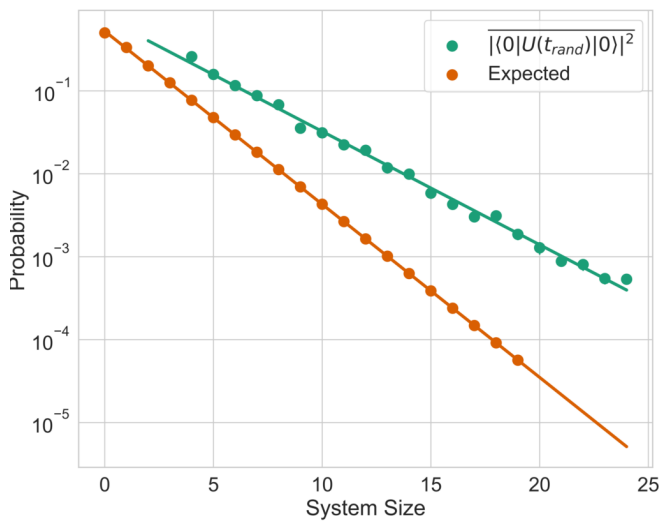


FIG. 5. Scaling of the averaged survival probability $\overline{S_p(t_{\text{rand}})}$ on a 1D chain as a function of system size. The simulated probability distribution is shown in teal, while the expected thermal value is shown in orange. Fits to an exponential decay form $f(n) = \exp(-\alpha n - \beta)$ are shown, with $(\alpha, \beta) = (0.314, 0.282)$ for the simulation and $(\alpha, \beta) = (0.481, 0.646)$ for the expected value.

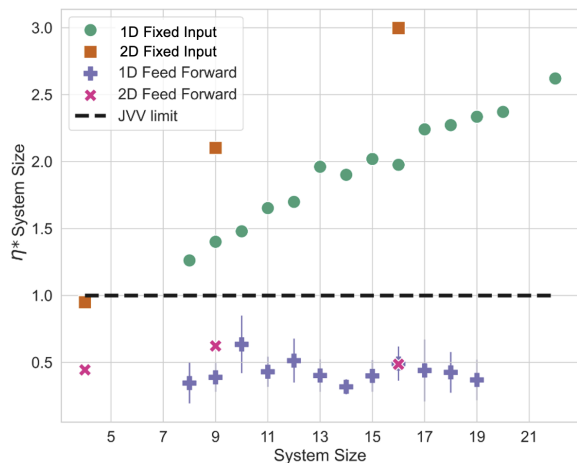


FIG. 6. Scaled non-uniformity $n\eta$ of RYDSAMP as a function of system size n . The dashed line illustrates $n\eta = O(1)$, required for a constant-factor approximation. Data is shown for both 1D chains and 2D uniform square grids for the FI and practical FF protocols. The practical FF data is averaged over ten trials.

the non-uniformity of the overall sample distribution of the practical FF. While strictly worse than the ideal FF procedure, the non-uniformity is below the JVV limit which allows us to perform the algorithm more efficiently albeit with a small finite error [16].

In Fig. 7, we show the behavior of η for the mixed distribution $\mathcal{D}(k)$ of the practical FF as a function of the total number of steps taken k , i.e. the number of different initial states taken. For the same 1D chain and

$|0\rangle^{\otimes n}$ input, we performed many runs of practical FF, whose outputs are shown. We see that, on average, η decreases with increasing k , but does not converge to a single point. There is an inherent bias in this sampling procedure as the distribution at each step is linked to the previous measurement outcome, but heuristically we see the overall bias decrease with number of steps. Also, η is not monotonous in k . One scenario that can cause this behavior is sampling that chooses scarred states [44, 45], which have an exceptionally high probability of returning to themselves. These states then become “attractors” that bias the output distribution, so that the process effectively reduces to the FI protocol. However, since the scarred states are few and exceptional, we expect that, as the system size grows, the overall probability of randomly choosing these detrimental states decreases.

Estimate of t_{min} and relation to the Thouless time

In Ref. [50], the authors argue that, for generic local Hamiltonians, the Thouless time is proportional to $t_{\text{Th}} \propto \frac{\mathcal{D}^{2/3}}{\Gamma} \sim \frac{e^{2cn/3}}{\sqrt{n}}$, where \mathcal{D} is the dimension of the Hilbert space $\mathcal{D} \propto e^{cn}$, Γ is the width of the local density of states and is related to the number of states directly coupled to the initial state (for a local Hamiltonian like the PXP model, $\Gamma \sim n$ [49]), and c is a constant. The authors also argue that, for chaotic evolutions under random GOE Hamiltonians, the Thouless time converges to a constant.

Fig. 8 shows the survival probability $S_p(t)$ for two 1D chains of lengths $n = 16, 24$. The characteristic feature associated with the Thouless time t_{Th} in the survival probability is the ramp-dip structure [50]. The minimum of this feature is seen in Fig. 8 to occur for $\Omega t \sim 1$ while

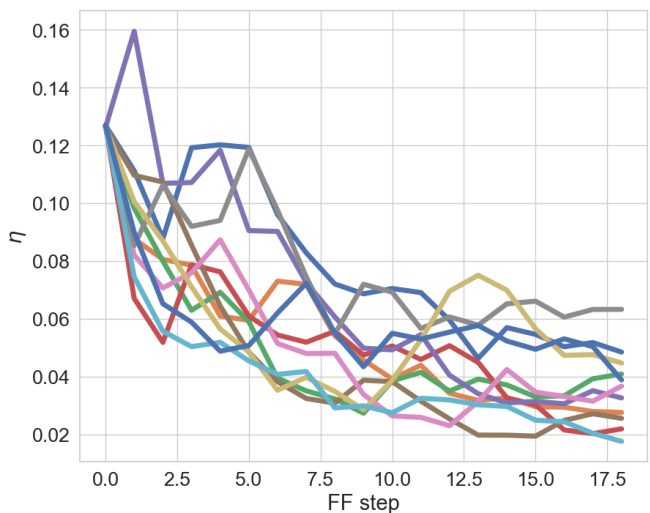


FIG. 7. Convergence of the non-uniformity η of the output distribution $\mathcal{D}(k)$ of the practical FF procedure as a function of the number of FF steps k for a 1D chain of size $n = 18$.

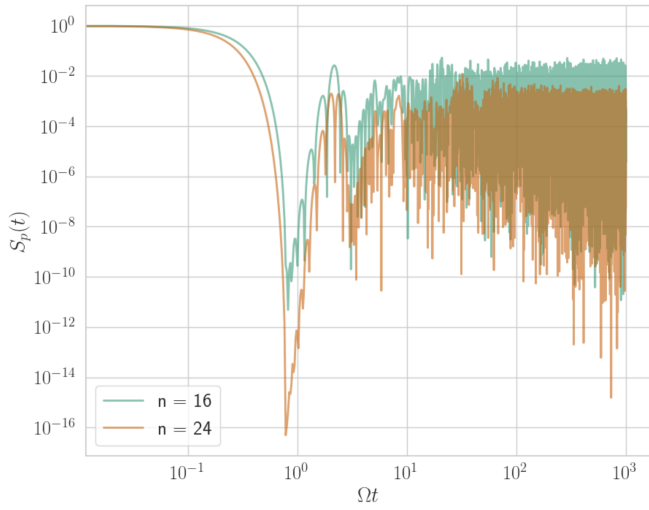


FIG. 8. The survival probability $S_p(t) = |\langle 0 |^{\otimes n} \mathcal{U}(t) | 0 \rangle^{\otimes n}|^2$ of the all zero state, with unitary evolution $\mathcal{U}(t) = \exp(-itH_{\text{Ryd}})$, for two 1D chains of length $n = 16$ and $n = 24$. The middle of ramp-dip structure can be observed around $\Omega t \sim 1$ while it ends at $\Omega t \sim 10$.

its end occurs roughly at $\Omega t \sim 10$ for both system sizes. Thus, we empirically set $\Omega t_{\text{min}} = 10$ in our protocol.